Contribution from the Department of Chemistry,
Princeton University, Princeton, New Jersey 08540

Anisotropic Exchange and Temperature-Dependent Electron Paramagnetic Resonance Line Width in One-Dimensional Copper(II) Complexes. 2. Magnetic Properties of $Cu(C_2O_4)\cdot{}^1/_3H_2O$

KENNETH T. McGREGOR and ZOLTÁN G. SOOS*

Received January 28, 1976 AIC600729

The temperature dependence of the X- and Q-band EPR line width, ΔH, of powder $Cu(C_2O_4)\cdot{}^1/_3H_2O$ is interpreted in terms of an anisotropic exchange $D_e = 2.5 \pm 0.5$ cm^{-1}. Such large D_e is consistent with the large isotropic exchange $J_0 = -130$ cm^{-1} obtained by analyzing static susceptibility data in terms of an infinite, one-dimensional, antiferromagnetic Heisenberg chain. The temperature dependence of ΔH is further evidence for a model of uniform magnetic dilution for treating exchange narrowing in paramagnets at low temperature ($kT \lesssim |J_0|$). The g values and the frequency dependence of ΔH are discussed in terms of magnetically inequivalent chains.

I. Introduction

Exchange coupling between copper(II) ions in discrete clusters and in n-dimensional arrays can usually be described by a spin Hamiltonian based on nearest-neighbor exchange interactions. For the one-dimensional (1d) case, the exchange Hamiltonian is

$$\mathcal{H}_{ex} = \sum_{n=1}^{N} \vec{S}_n \cdot \mathbf{J}_n \cdot \vec{S}_{n+1} \tag{1}$$

and represents nearest-neighbor exchange for N copper(II) sites. The crystal is then built up of such infinite strands. The interaction $\mathbf{J}_n$ is written in tensor form in order to include the possibility of anisotropic exchange. Although, in most cases, the bulk magnetic properties[1] (susceptibility, magnetization, specific heat, etc.) of copper(II) systems are well accounted for by the isotropic exchange parameter J_0, a number of EPR studies on magnetic clusters[2] clearly indicate the existence of anisotropic terms. Antisymmetric exchange is forbidden by symmetry in the few copper chains considered.

The role of anisotropic exchange in the spin dynamics of low-dimensional paramagnets has been emphasized[3,4] recently, since it provides an important relaxation mechanism in 1d copper(II) crystals. Anisotropic exchange between adjacent exchange-coupled sites n and $n + 1$ can be expressed as

$$\mathcal{H}_{ae} = \vec{S}_n \cdot \mathbf{D}_e \cdot \vec{S}_{n+1} \tag{2}$$

where $\mathbf{D}_e$ is a symmetric and traceless tensor which transforms like the magnetic dipole–dipole interaction. The pseudodipolar term arises from a combination of the isotropic exchange and the spin–orbit interaction and is estimated to be of the order[5]

$$D_e \sim (\Delta g/g)^2 J_0 \tag{3}$$

where Δg describes the orbital contribution to the ground-state functions.

The relaxation of the spin system produced by terms like (2) can be estimated from the EPR line width[6]

$$\Gamma \sim M_2/\nu_{ex} \tag{4}$$

Here Γ is the half-width at half-height of the resonance absorption, M_2 is the second moment of the resonance line, and ν_{ex} is the effective exchange frequency. At high temperatures, ν_{ex} is of the order J_0/h and, in the absence of other relaxation mechanisms, $M_2 \sim D_e^2$. Clearly from (3) and (4), in the limit of very large J_0, the EPR line width should be dominated by (2) and becomes proportional to $(\Delta g/g)^4 J_0$. This is, in effect, an exchange-broadening mechanism.

The linear-chain copper(II) crystals[4] whose spin dynamics have been previously characterized have isotropic exchange parameters of ~ 10 cm^{-1}. Since $\Delta g/g \approx 0.1$ in these crystals, the anisotropic exchange fields are predicted by (3) to be $\sim 10^3$ G, which is comparable to the dipolar fields calculated from crystal structure data. This prediction was confirmed by the observed EPR line width data.[4] In order to test the validity of (3) in the limit of large J_0, we undertook EPR studies on $Cu(C_2O_4)\cdot{}^1/_3H_2O$. The magnetic susceptibility[7] of this material, whose structural characterization awaits the growth of single crystals, is shown below to exhibit 1d exchange, with $J_0 \approx 130$ cm^{-1}. The anisotropic exchange (3) should consequently be an order of magnitude larger, or about 10^4 G. Such large isotropic exchange and the concomitant large D_e, which is an order of magnitude larger than any dipolar field for copper ions separated by 2.5–4 Å, allows in this case a reasonably detailed picture of the spin dynamics through the temperature and field dependence of the EPR line width of the powder.

We report here EPR studies on powder $Cu(C_2O_4)\cdot{}^1/_3H_2O$, as a function of both temperature and frequency. The large isotropic 1d exchange of $J_0 \approx 130$ cm^{-1} leads naturally to low-temperature spectra in the region $kT < J$. Standard theories[8] of magnetic resonance are based on the opposite limit of $kT >> J$. The study of anisotropic exchange in a large-J system consequently requires a more detailed application of the theory of uniform magnetic dilution,[6a,9] which was originally applied to regular and alternating organic ion–radical crystals.[10] In contrast to large-J regular organic chains, however, the static susceptibility of $Cu(C_2O_4)\cdot{}^1/_3H_2O$ closely follows, as shown in section IVA, the theoretical result for a 1d antiferromagnetic chain. A far more complete analysis of the anisotropic exchange contribution to the spin dynamics is then possible.

II. Experimental Section

A. Preparation. Powdered samples of hydrated copper(II) oxalate were prepared by mixing aqueous solutions of $CuSO_4\cdot 5H_2O$ and $H_2C_2O_4$ in stoichiometric proportions. This procedure results in the immediate precipitation of a very finely divided light blue powder. The powder was dried at ~110 °C for several days. Immediately prior to chemical analysis or to any magnetic measurement, the material was redried at ~110 °C in vacuo for 2 h. Anal. Calcd for $Cu(C_2O_4)\cdot{}^1/_3H_2O$: C, 15.25; H, 0.43; Cu, 40.33. Found: C, 15.50; H, 0.69; Cu, 40.67.

B. EPR Spectra. All EPR spectra were obtained with standard Varian spectrometers using 100-kHz magnetic field modulation. Spectra were recorded at temperatures in the range 13–333 K with 9.18-GHz (X-band) irradiation and in the range 100–300 K with 35.4-GHz (Q-band) irradiation. For the X-band measurements, sample temperature was achieved and controlled with Varian V6040 and Air Products Model OC-20 cryogenic temperature controllers. The accuracies of these temperature measurements are estimated to be ±3 K for $T < 100$ K and ±5 K for $T \gtrsim 100$ K. The low-temperature Q-band spectra were obtained by using the ambient

temperatures of various cryogenic baths with an estimated accuracy of ±10 K.

III. Analysis of Exchange-Narrowed Line Widths

A. Magnetic Resonance Theory for Strong Exchange. The general theories[8] of magnetic resonance which are applicable to exchange-coupled systems depend heavily on the high-temperature limit. When kT exceeds any exchange energy J or magnetic term in the spin Hamiltonian, then the detailed energy spectrum for the interacting spins is not required and the partition functions reduce to the number of available spin states. These approximations are fundamental to the general treatments[8] of paramagnetic systems, since they neatly avoid the far more difficult problem of finding energy levels and their degeneracies. One-dimensional systems remain paramagnetic for $T > 0$ K, although in practice weak interchain contributions result in ordered (3d) states at sufficiently low temperatures. Nevertheless, it is evident that low-dimensional paramagnetic systems afford convenient models for the case of $J \gtrsim kT$, without having ordered spins.

The extension of exchange-narrowing theory or other EPR results to such strong interactions has been principally demonstrated in dimerized organic free-radical crystals.[6a,10a] The occurrence of successively large and small isotropic exchange parameters J and J', respectively, in (1) naturally leads to a collection of dimers whose interactions go as J'. For $S = {}^1/_2$ and $J < 0$, each dimer has a ground singlet and an EPR-active triplet state at $2J$. The thermal density of triplets is in the limit $J' = 0$

$$\rho_t(T) = [1 + {}^1/_3 \exp(-2J/kT)]^{-1} \tag{5}$$

and the static susceptibility is given by a concentration $\rho_t(T)$ of noninteracting triplets. The J' terms account for triplet motion along the chain, as required by the exceptionally narrow EPR lines in the solid. Triplet-spin excitons have also been identified in dimerized Cu(II) crystals,[10b] again through their characteristic fine structure splitting. The extension of standard EPR methods to dimerized chains thus primarily requires an explicit treatment for the density $\rho(T)$ of magnetically active spins.

A similar approach, again without explicitly considering the detailed energy spectrum, has been suggested for regular chains.[9] The physical picture is now more complicated, however, and the present application to $Cu(C_2O_4)_2 \cdot {}^1/_3H_2O$ has the important advantage that the susceptibility is in fact found to follow the result for a 1d Heisenberg antiferromagnetic chain. When $J >> kT$, antiferromagnetic exchange along the chain tends to orient adjacent spins antiparallel. Equally strong exchange constants in a regular chain then lead to segments, of length $\xi(T)$, of correlated spins. Such short-range order[11] (SRO) effectively removes spins from either EPR or χ measurements, since they cannot be reoriented by microwave or thermal energies, respectively. The effective density of spins $\rho(T)$ in a regular chain must decrease with temperature since there is increasing SRO. Two essentially identical definitions of $\rho(T)$ are possible.

The first is based on an analogy with alternating chains and is simply[6a]

$$\rho(T) = \chi(T)/\chi_c = \frac{3kT\chi(T)}{Ng^2\beta^2} \tag{6}$$

where $\chi(T)$ is the observed susceptibility and χ_c is the Curie-law result for an equivalent number of (noninteracting) spin ${}^1/_2$ moments. Physically, (6) corresponds to the assumption that large J reduces $\chi(T)$ from its Curie-law value, but with the resulting spins still noninteracting. This idea can be used whenever $\chi(T)$ data are available. When $\chi(T)$ corresponds to a 1d Heisenberg antiferromagnetic chain, the spin density (6) reduces to

$$\rho_H(T) = 4xf(x) \tag{7}$$

where $x = kT/J_0$ and values for $f(x)$ have been tabulated by Bonner and Fisher.[12] ($f(x)$ varies between 0.05 and 0.07 for x between 0 and 2.5.) The region $kT \lesssim J$ thus corresponds, in the approximation of noninteracting spins, to an excitation density $\rho_H(T)$ that is almost linear in T. By contrast, $\rho_t(T)$ in (5) is exponential for $kT < J$. The phenomenological definition (6) applies to any type of antiferromagnetic interaction that reduces $\chi(T)$, whereas $\rho_H(T)$ in (7) is the special case for 1d Heisenberg antiferromagnetic chains.

The second approach to $\rho(T)$ in a regular chain is based on the correlation length[11] $\xi(T)$. Clearly, any segment of *odd* length has a net $S = {}^1/_2$ and can give an EPR signal. Even segments, on the other hand, have singlet ground states. Their energy gaps, of order J_0/n for $2n$ spins, lead[12] to vanishing $\chi(T)$ at sufficiently low T. Since even and odd segments are in dynamic equilibrium and are constantly forming and dissolving through thermal fluctuations, the effective spin density is

$$\rho_\xi(T) = [2\xi(T)]^{-1} \tag{8}$$

and corresponds to the concentration of odd-length segments. The physical picture for $\rho_\xi(T)$ is clear. The main drawback is that the correlation length $\xi(T)$ is relatively difficult to compute or to measure. (It can be found, for example, through inelastic neutron diffraction.[13]) However, results[11b] are available for the classical 1d Heisenberg chain and lead to $\xi(T) \approx 2J/kT$ in units of the lattice spacing. Hence (8) yields a linear increase with T, as did $\rho_H(T)$ in (7). Even the numerical coefficients of kT/J compare favorably, since (8) gives 0.25 while (7) leads to 0.24 at low T.

Both methods provide a way of reducing the effective number of EPR-active spins when $kT \lesssim J$. The phenomenological approach (6) or (7) is more precise, since the observed $\chi(T)$ is used. The more detailed physical picture afforded in (8) by taking the inverse of the correlation length then emphasizes how the build-up of dynamic SRO reduces the spins available for EPR. Either approach leads to straightforward modifications of the infinite-temperature results, since strong exchange is approximated by a density effect. In particular, we still have kT large compared to the purely magnetic interactions and can approximate, as before, all spin partition functions by the number of states.

B. The High-Temperature Limit. The calculation[8] of exchange-narrowed line widths in the high-temperature region generally begins with a spin Hamiltonian of the form

$$\mathcal{H} = \mathcal{H}_0 + \mathcal{H}' \tag{9}$$

where $\mathcal{H}_0$ consists of the Zeeman and exchange interactions and $\mathcal{H}'$ represents perturbations such as magnetic dipole–dipole interactions, anisotropic exchange, and hyperfine interactions. In the case of nearly 1d exchange, $\mathcal{H}_0$ may be written as

$$\mathcal{H}_0 = \sum_{n=1}^{N} [\beta \vec{H} \cdot \mathbf{g}_n \cdot \vec{S}_n - 2J_0 \vec{S}_n \cdot \vec{S}_{n+1} - \sum_{n'=1}^{z} J'_{nn'} \vec{S}_n \cdot \vec{S}_{n'}] \tag{10}$$

where the sum is carried out over the N magnetic sites in the crystal. The symbols in (10) have their usual meanings, with the isotropic interactions of (1) given by a strong intrachain exchange J_0 and a much weaker interchain coupling $J'_{nn'}$. Thus n' is a copper(II) site in a neighboring chain and we postulate z neighboring chains.

The basic quantity of interest in calculating the exchange-narrowed line width is the correlation function[8] of the local magnetic fields

$$\psi(\tau) = \langle \Delta\nu(\tau)\Delta\nu(0)\rangle \tag{11}$$

We assume that all of the paramagnetic sites have a common **g** tensor in (10). Then $\Delta\nu$ represents small deviations from the Larmor frequency $2\pi\nu_0$ ($=\hbar^{-1}\beta|\mathbf{g}\cdot\tilde{H}_0|$), which arise from local field perturbations of the energy spectrum. The time dependence (fluctuations) of $\Delta\nu(\tau)$ can relax the spin system. The local fields are produced by $\mathcal{H}'$, while their time dependence is governed by $\mathcal{H}_0$. The magnitude of the local fields is given by the second moment M_2

$$M_2 \equiv \psi(0) = \langle \nu(0)^2\rangle \tag{12}$$

As shown in detail elsewhere,[8,14] the local field correlation function can be written in the form

$$\langle \Delta\nu(\tau)\Delta\nu(0)\rangle = \sum_{\gamma=0}^{2} g_\gamma(\tau)\cos(2\pi\nu\gamma\tau) \tag{13}$$

where $g_\gamma(\tau)$ is the correlation function for that part of the perturbation which causes a change $\Delta M \equiv \gamma$ in the total quantum number M of the spin system. The form of $\psi(\tau)$ given by (13) is advantageous since a clear distinction is made between the secular ($\Delta M = 0$) and nonsecular ($\Delta M \neq 0$) terms of the perturbation $\mathcal{H}'$. Also, in (13), the time dependence of $\psi(\tau)$ resulting from the Zeeman part of $\mathcal{H}_0$ is contained explicitly in the cosine term. The correlation functions $g_\gamma(\tau)$ then depend only on $\mathcal{H}_{ex}$. In the limit of strong exchange modulation $J_0 >> \mathcal{H}'$, the EPR absorption spectrum can be expressed[8] as

$$I(\nu - \nu_0) = \mathrm{T}\{\exp[-t\textstyle\int_0^\infty \psi(\tau)\,d\tau]\} \tag{14}$$

where T indicates the frequency Fourier transform at frequency ν. The form (14) leads to a Lorentzian profile for $I(\nu - \nu_0)$. The derivation of (14) assumes that $\psi(\tau)$ decays rapidly in comparison to Γ^{-1}; i.e., the local fields are essentially averaged to zero by the exchange modulation after times $\sim h/J << \Gamma^{-1}$. This assumption can be in serious error for purely 1d exchange.[6b] Recent theoretical studies[6b,15] suggest that $\psi(\tau)$ is governed by spin diffusion at long times. This argument leads to the divergence[15] of the integral in (14) for 1d exchange since $\psi(\tau) \propto \tau^{-d/2}$ for diffusional decay. However, it has been shown[6b,16] that relatively small interchain interactions are sufficient to "cut off" the slow diffusional decay of $\psi(\tau)$ and to suppress the 1d line shape. The approximation (14) can be justified whenever the observed EPR absorption is Lorentzian.[16]

When the absorption profile $I(\nu - \nu_0)$ is Lorentzian, the exchange-narrowed line width is given by the Fourier components of (13)

$$\Gamma = \sum_{\gamma=0}^{2} M_2^{(\gamma)} f(\gamma\nu) \tag{15}$$

In the case of interest here, with $J_0 >> h\nu_0$ and at high temperature, we have $f(\gamma\nu) \approx f(0) \approx h/J$; this leads to the order-of-magnitude estimate (4). As already mentioned, exchange in highly 1d systems leads to important corrections in $f(0)$, whose divergence in the limit of rigorously 1d exchange is responsible for non-Lorentzian EPR profiles, as first observed[17] in $(CH_3)_4NMnCl_3$. In less completely 1d systems such as $Cu(NH_3)_4PtCl_4$, with Lorentzian EPR absorptions, the secular component $f(0)$ is enhanced by a factor of $(1 + \varkappa)$, with $\varkappa \approx 1$. Such enhancements are important in single-crystal line width studies.[4,16] In the present case of a powder sample, it is doubtful that such 1d enhancement of the secular components could be demonstrated. Further, for large J_0, the nonsecular ($\gamma \neq 0$) components in (15) contribute fully, and no enhancement occurs for them.

Explicit formulas for the various contributions $M_2^{(\gamma)}$ in (15) have been derived for the case of dipolar,[8] of hyperfine,[16] and of anisotropic exchange[4] perturbations. For large J_0, the latter is by far the dominant contribution and yields for $S = {}^1/_2$

$$h^2M_2 = 3D_e{}^2S(S+1)(1+\cos^2\varphi) = 3D_e{}^2 \tag{16}$$

upon taking the powder average of φ, the angle between the principal z direction of (2) and the applied field. In (16), the full nonsecular second moment $M_2 = M_2^{(0)} + M_2^{(1)} + M_2^{(2)}$ is used, as required when J_0 exceeds the Larmor frequency $2\pi\nu_0$.

The final step in applying (15) is to find the Fourier components $f(\gamma\nu)$. Formal analyses[14] relating $f(\gamma\nu)$ to various two- and four-spin correlation functions are given elsewhere. Although in practice the spin dynamics require several approximations, the rough estimate of $f(0) \approx h/J$ used in (4) can be significantly improved. The anisotropic exchange (2) leads to four-spin correlation functions which, as in the case of dipolar broadening, are further simplified by decoupling. The most important contributions[16] to $f(\gamma\nu)$ then involve Fourier components of $C^2(t)$, where $C(t) = 4\langle S_i^z(t)S_i^z(0)\rangle$ is the normalized two-spin autocorrelation function and is central to the description of spin dynamics.

There are several approaches[18,19] to computing $C(t)$, including computer simultations[11c] for finite systems. We adopt here the Blume–Hubbard[18] result for $C(t)$. Their model is based on the root-mean-square exchange, $\hat{J}^2 = \sum_j J_{ij}{}^2$, where the sum is over the j neighbors of site i. Nearest-neighbor exchange $2J_0$ between adjacent sites in a 1d system gives $\hat{J} = 2(2^{1/2}J_0)$ when interchain contributions are neglected. The Fourier components[16] of $C^2(t)$ are

$$f(y) = \frac{4}{3\hat{J}}\frac{y}{\sinh y}[1 + (y/\pi)^2] \tag{17}$$

with $y = 2\pi^2\nu/\hat{J}$. Since $\hat{J} = 2(2^{1/2}J_0)$ is far larger than $h\nu_0$, we have $y \approx 0$ in (19) for all Fourier components $f(\gamma\nu)$ in (15). The nonsecular terms then contribute fully and $f(\gamma\nu) \approx 4/3\hat{J}$ for $\gamma = 0, 1, 2$. The exchange-narrowed line width (15) then reduces to

$$\Gamma = 4D_e{}^2/\hat{J} = 2^{1/2}D_e{}^2/J_0 \tag{18}$$

when the anisotropic exchange contribution (16) dominates M_2.

The expression (18) is valid at high temperature and must still be modified for the case $kT \lesssim J_0$. The main purpose of sketching the derivation of (18) and of mentioning the types of approximations that are involved is to emphasize the large number of special cases of exchange narrowing. In the qualitative general formula (4), both the local fields that contribute to M_2 and the dynamical processes described by $\nu_{ex} \approx J/h$ are amenable to more complete analysis. Detailed line width studies, for example in single crystals, clearly require such improved theoretical treatments. Different special cases of exchange narrowing can be expected for different ordering of such quantities as J_0, $h\nu_0$, J', and dipolar or hyperfine fields.

C. Extension to Low Temperature ($kT \lesssim J$). A rigorous treatment of the temperature dependence of Γ would require evaluation of the resonance line moments and spin correlation functions of (16) in terms of the partition functions of the system based on the detailed (and usually unknown) energy spectrum of the interacting spins. We instead give here an approximate approach based on the density of free spins $\rho(T)$ as outlined in section IIIA. The dilution of free spins by SRO as a function of temperature is used to establish the temperature dependence of both M_2 and the spin correlations.

The second moment observed for a system of noninteracting spins of density $\rho(T)$ can be evaluated by considering the lattice to be diluted with nonmagnetic sites. This presents an interesting situation, since various terms in $\mathcal{H}'$ are affected

differently by such dilution. Kittel and Abrahams[20] have treated the case of the dipolar field M_2^d in the presence of magnetic dilution. They found that except for very dilute systems ($\rho < 0.01$)

$$M_2^d(\rho) = \rho M_2^d \tag{19}$$

where ρ is the fraction of magnetic sites. This dependence arises from the fact that the dipolar field of any reference site depends on the probability that a neighboring site is magnetic. The dipolar field is not restricted to nearest neighbors and, in a paramagnetic sample, there are roughly equal numbers of up and down spins. All neighbors contribute, with the magnitude of the interaction falling off as r^{-3}, and there is considerable cancelation. The net result is that M_2 goes as ρ. This is not the case, however, for the anisotropic exchange field,[21] which is a short-range interaction. As seen from (2) and (3), the local fields arising from (2) depend on the probability that pairs of sites are magnetic. This gives

$$M_2^{ae}(\rho) = \rho^2 M_2^{ae} \tag{20}$$

Finally, since the hyperfine contribution arises from single sites, M_2^{hfs} is independent of ρ.

The temperature dependence of $\nu_{ex}^{-1} = f(0)$ is estimated, following the model of triplet spin excitons,[10] according to the collision frequency of the free spins. That is, $\nu_{ex}(\rho)$ has the form[9]

$$\nu_{ex}(\rho) = \rho \nu_{ex} \tag{21}$$

where ν_{ex} represents the high-temperature limit and the EPR-active spins neither attract nor repel each other. Now substitution of (19), (20), and (21) into (15) leads to two quite different possibilities. If $M_2^d >> M_e^{ae}$, as in organic ion-radicals where $M_2^{ae} \approx 0$, then the effects of $\rho(T)$ on M_2 and ν_{ex} cancel and a temperature-independent line width is predicted. The very gentle temperature and pressure dependence of Γ in regular organic 1d systems was an early indication for such a picture of uniform magnetic dilution.[6a,22] In $Cu(C_2O_4)\cdot{}^1/_3H_2O$, on the other hand, we have $M_2^{ae} >> M_2^d$ (vide infra) so that there is a net dependence of $\rho(T)$. The exchange-narrowed (Lorentzian) resonance has a peak to peak derivative width ΔH ($=2\Gamma/3^{1/2}$)

$$\Delta H(T) = 2[6^{1/2} D_e^2 \rho(T)/3J_0] \tag{22}$$

The line width is then predicted to go as the free spin density or, for a 1d Heisenberg chain, approximately as T.

The form (21) for $\nu_{ex}(\rho)$ ($\sim \rho J/h$) has been demonstrated[10] for the alternating-chain (triplet exciton) systems. Although the precise form for $\nu_{ex}(\rho)$ in regular chains is not known, we adopt (21) for analyzing $Cu(C_2O_4)\cdot{}^1/_3H_2O$. It should be emphasized, however, that (21) is best regarded as an approximation without rigorous derivation. Moreover, since $\nu_{ex}(\rho) \to 0$ as $\rho \to 0$, the occurrence of a single-narrowed line is expected only when $\nu_{ex}(\rho) >> M_2$. In the opposite limit of $\nu_{ex} < M_2$, resolved EPR lines are observed.

IV. Results

A. Magnetic Susceptibility. The temperature dependence of the bulk magnetic susceptibility of $Cu(C_2O_4)\cdot{}^1/_3H_2O$ in the region 80–350 K has been reported independently by several groups.[7] The overall temperature dependences of all the data are similar; a very broad maximum is observed around 260 K. The major discrepancy between the different data sets is the absolute magnitudes of the susceptibilities. The maximum values range from 620×10^{-6} to 700×10^{-6} cgsu after correction for the diamagnetism of the constituent atoms.

Initial attempts[7a,b] to interpret the observed susceptibility in terms of an exchange interaction has ruled out the possibility of discrete pairs of exchange-coupled copper(II) ions, since

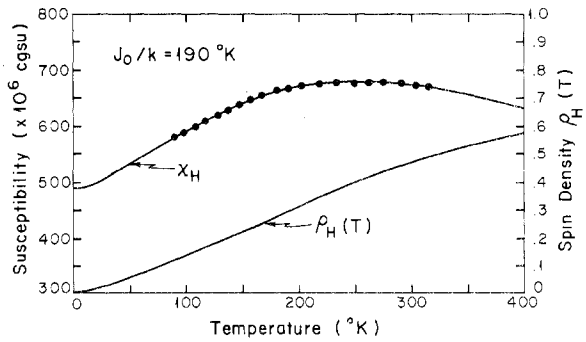

Figure 1. Bulk magnetic susceptibility and free spin density of powder $Cu(C_2O_4)\cdot{}^1/_3H_2O$. The experimental points (•) are representative of the data given in ref 7. The solid curves are based on the Bonner-Fisher result for a 1d antiferromagnetic interaction with $J_0/k = 190$ K. The free spin density is computed from eq 7.

$\rho_t(T)$ in (5) does not fit the $\chi(T)$ data. Subsequently, Jotham[23] has shown that the data are consistent with an extended interaction and are best described by a 1d Heisenberg Hamiltonian. However, the exchange parameter reported by Jotham differs substantially from that inferred from the qualitative features of the data; i.e., $T_{max} \approx 260$ K suggests[12] an exchange parameter $J_0/k \approx 200$ K whereas Jotham[23] derived the value $J_0/k \approx 260$ K. In order to resolve this discrepancy and to confirm the 1d model for the exchange interaction, we have carried out a least-squares analysis of the reported data. All of the data sets can be described by the 1d Heisenberg interaction given in (10) with $J' = 0$

$$\chi_H = \frac{Ng^2\beta^2}{|J_0|} f(x) + N\alpha \tag{23}$$

Here $f(x)$ is the tabulated function,[12] already introduced in the definition $\rho_H(x)$ in (7). The best fit to (23) was established by minimization of the function

$$F = \sum_i [\chi_i(T) - \chi_H(T)]^2 \tag{24}$$

by varying g and $|J_0|$. The TIP of copper(II) was fixed at $N\alpha = 60 \times 10^{-6}$ cgsu.

As expected from the varying magnitudes of the susceptibilities between data sets, the g values obtained from the fitting process vary significantly and are in the range 1.95–2.13. On the other hand, the exchange parameters J_0/k obtained are very nearly the same for all of the data and are in the range 180–195 K. This amounts to a relatively minor dependence of J_0 on the particular data set. A representative[7a] set of susceptibility data is shown in Figure 1, along with the best fit to (23). The calculated curve in Figure 1 was generated with $|J_0/k| = 195$ K and $g = 2.13$. Comparable fits were achieved for all of the data, again with similar exchange parameters. The spin density $\rho_H(T)$ for $J_0/k = 195$ K is also shown in Figure 1. As anticipated in section IIIA, $\rho_H(T)$ is nearly proportional to T in the low-temperature region of $kT < 2J_0$.

Preliminary susceptibility measurements in the region 4.2–70 K have been made by Hatfield.[24] These low-temperature results are consistent with the 1d exchange model. In particular, there is no 3d ordering down to at least 4.2 K, which consequently sets an upper bound on any interchain exchange interactions J'.

B. EPR Spectra. The temperature dependences of the X- and Q-band EPR spectra are illustrated in Figures 2 and 3, respectively. The experimental spectra correspond to powdered sample measurements and are displayed in digital form. As seen from Figures 2 and 3, the observed profiles have a marked temperature dependence. The spectra which show the most

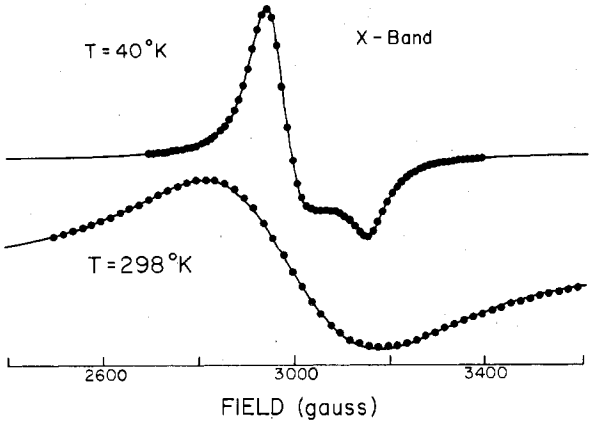

Figure 2. Temperature dependence of the X-band spectra. The experimental spectra (•) are for $\nu = 9.18$ GHz at $T = 40$ and 300 K. The calculated spectra (–) were generated with the best least-squares parameters: $g_z = 2.08$, $g_x = 2.19$, $g_y = 2.22$, and $\Delta H_X = 60$ and 330 G for $T = 40$ and 300 K, respectively.

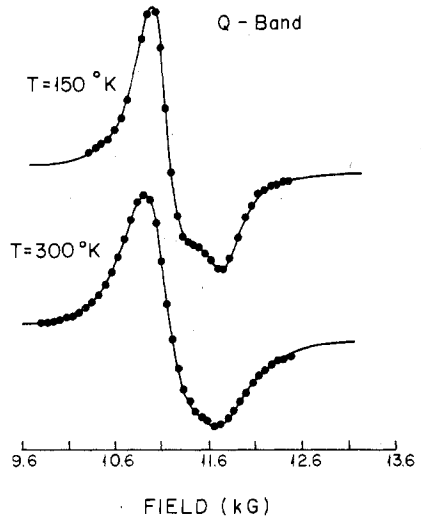

Figure 3. Temperature dependence of the Q-band spectra. The experimental spectra (•) are for $\nu = 35.4$ GHz at $T = 150$ and 300 K. The calculated spectra (–) were generated with the best least-squares parameters: $\Delta H_0 = 280$ and 400 G for the $T = 150$ and 300 K, respectively.

structure correspond to $T \simeq 40$ K at X band and to $T \simeq 150$ K at Q band.

Since the measurements were made on powdered samples, the spin Hamiltonian parameters cannot be accurately determined directly from the observed spectra. However, the necessary information can be extracted by computer simulations. The parameters to be determined are the g values, the line width, and an arbitrary intensity. Our simulation procedure employed a fully anisotropic **g** tensor and an average line width parameter. The simulated spectra in Figures 2 and 3 were generated by standard methods[25] using a Lorentzian profile for the line shape. The parameters were determined by fitting the calculated spectra to the observed data using the least squares method described above for $\chi(T)$. The 40 K X-band spectrum was used initially to determine the g values, since it shows the most structure and should therefore be the most sensitive to g value variation. All other X-band spectra were fitted by holding the g values constant and allowing the line width and intensity to vary. In general, very good agreement between the calculated and experimental data was achieved over the entire temperature range. The Q-band data were treated in a similar way and with comparable results. Identical g values were obtained at both frequencies.

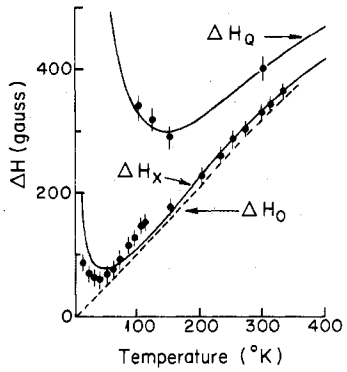

Figure 4. The temperature dependence of ΔH. The experimental data (•) were determined from simulations like those shown in Figures 2 and 3. The error estimates were derived from the least-squares procedure. The solid curves were generated with eq 26 where $A = 750$ G and $B = 217 \times 10^{-9}$ G^{-1}. The field-independent line width ΔH_0 was determined from eq 25; see text.

Therefore, within the sensitivity of the measurement, the g values are frequency and temperature independent at $g_z = 2.08$ (1), $g_x = 2.19$ (1), and $g_y = 2.22$ (1). In contrast, the line width ΔH is both temperature and frequency dependent. The X-band line width ΔH_X varies between 60 and 330 G between 13 and 330 K, with a minimum value at 40 K. The Q-band line width ΔH_Q varies between 280 and 400 G in the region 100–300 K with a minimum at $T \simeq 150$ K. Assuming an H_0^2 dependence of the line width on frequency as discussed in section V, the frequency-independent line width ΔH_0 can be calculated according to

$$\Delta H_0 = \frac{p^2 \Delta H_X - \Delta H_Q}{p^2 - 1} \tag{25}$$

where $p = \nu_Q/\nu_X = 35.4/9.18$. The temperature dependences of ΔH_X, ΔH_Q, and ΔH_0 are shown in Figure 4, along with the calculated line widths described in the next section. The high-temperature data ($T \geq 150$ K) were used to calculate ΔH_0 and then extrapolated to lower temperatures.

V. Discussion

A. Temperature Dependence of ΔH. As seen from Figure 1, the observed susceptibilities agree very well with the Bonner–Fisher[12] result for the 1d antiferromagnetic exchange model with $|J_0| = 130$ cm^{-1}. With an exchange parameter of this magnitude, the dipolar and hyperfine contributions to the EPR line width must be extremely small compared to the observed line widths. The dipolar fields calculated from a point-dipole model (maximum value) with an optimum copper–copper separation (~2.5 Å) yield a dipolar contribution to the line width (4) of ~1 G. The hyperfine contribution is even smaller.

We therefore expect the infinite-temperature second moment to be given by the anisotropic exchange term to a very good approximation. Furthermore the temperature dependence for $T \geq 150$ K is in line with the predictions of (22). However, it is clear that (22) cannot account for all of the experimental data. Extrapolation of the high-temperature X-band data ΔH_X (momentarily neglecting the increase in ΔH_X at low temperatures) to zero temperature ($\rho = 0$) yields a nonzero intercept of ~30 G. This is much too large to be attributed to dipolar contributions and suggests the presence of an additional broadening mechanism. This is also apparent from the frequency dependence of the data. Such frequency dependence arises[6] naturally from the presence of additional chains that are perhaps crystallographically equivalent but have different relative orientations of their $\mathbf{g}_n$. The resonance lines of these magnetically nonequivalent sites are not resolved but are averaged into a single line by small interchain in-

teractions J'. The resulting resonance line is given by an average g value corresponding to the arithmetic mean of the individual g values. The occurrence of magnetically inequivalent chains is also suggested by the observed g values,[26] as discussed below. This contribution to M_2 is proportional to $(g_n - g_{n'})^2\beta^2H_0^2$. The H_0^2 contribution to the line width ΔH can be substracted, as shown in (25), to obtain the frequency-independent line width ΔH_0. As seen from Figure 4, ΔH_0 extrapolates to zero at zero temperature, in qualitative agreement with the $\rho(T) \rightarrow 0$ limit of the line width formula (22).

While the H_0^2 contribution to M_2 is independent of ρ, the exchange-narrowed line width is not. The interchain exchange J' leads to interchain motion of $\nu'_{ex} \approx J'/h$. As the probability of magnetic sites on adjacent chains decreases at low temperature, ν'_{ex} also decreases as $\rho\nu'_{ex}$. This approximation has already been discussed in connection with (21) for intrachain modulation. The resulting line width formula

$$\Delta H(T) = A\rho(T) + BH_0^2\rho^{-1}(T) \tag{26}$$

then generalizes (22) to the case of magnetically inequivalent chains. The two adjustable parameters A and B are for the present case with ΔH in hertz

$$A = 2(6^{1/2}D_e^2/3J_0)$$
$$B = (g_n - g_{n'})^2\beta^2/zJ'h^2 \tag{27}$$

where, as indicated in (10), there are z neighboring chains. The first term in (26) is approximated by the large D_e contribution expected from (3) for large J_0, while the second, frequency-dependent term reflects the postulated occurrence of magnetically inequivalent chains in $Cu(C_2O_4)\cdot{}^1/_3H_2O$.

The solid curves in Figure 4 were generated with (26) from parameters determined by a least-squares procedure using *all* of the data. The value for D_e obtained from (27) is 2.5 ± 0.5 cm^{-1}. This is in good agreement with (3) for $\Delta g/g \approx 0.1$ and $J_0 = 130$ cm^{-1}. A precise value for the interchain interaction cannot be determined from the powder data but an upper limit of $zJ' \lesssim 4$ cm^{-1} is suggested by the observation that $(g_n - g_{n'})/g$ is unlikely to exceed 0.2 for Cu(II) ions. The observed temperature dependence in Figure 4 is adequately accounted for by (26).

B. Magnetically Nonequivalent Chains. The observed g values have some additional structural implications. The values determined from the simulations correspond to the crystal values and are not necessarily those of discrete molecular units.[6,26] The observation that $g_z < g_x \sim g_y$, if attributed to a discrete molecular complex, suggests a d_{z^2} ground-state function; however, the value of $g_z = 2.08$ is too large for this case. Also, the coordination environment necessary to produce a d_{z^2} ground state is essentially impossible to achieve with the known empirical formula of the material. It is much more likely that the oxalate coordination leads to a primarily $d_{x^2-y^2}$ ground-state function. In this case, the observed values can be obtained in either or both of the following ways. The nonequivalent sites could be within the strongly coupled chain and/or in magnetically nonequivalent chains. The former situation would not produce the observed frequency dependence, while the latter arrangement would. Also, a simple calculation shows that the principal z directions of the nonequivalent sites must be $\sim 90°$ apart which tends to rule out the former arrangement.

Two types of structures have previously been suggested[7a] for copper oxalate. One is based on a ribbon-type arrangement of square-planar oxalate groups bound to adjacent copper(II) ions. The other is based on the adjacent ions being bridged by two different oxalate groups similar to the type of bridging found in copper acetate monohydrate, only in this case forming a linear chain. Although the latter structure is consistent with the relatively large exchange interaction observed, the former structure is more consistent with the EPR data. The present data cannot make a clear distinction between the two structures but emphasizes the need for single crystals.

C. Summary. The bulk magnetic susceptibility and EPR spectra of powdered samples of $Cu(C_2O_4)\cdot{}^1/_3H_2O$ are well accounted for by the nearest-neighbor exchange interactions of (1). The bulk susceptibility data are in good agreement with the results of Bonner and Fisher for a purely Heisenberg 1d model with $J_0 = -130$ cm^{-1}. The relatively large magnitude of J_0 and the 1d nature of the interaction presents a situation where paramagnetic resonance studies can be carried out over an extended temperature region with $kT \lesssim J$. The high-temperature EPR line width data are consistent with an anisotropic exchange interaction of the order predicted by (3), which at X band is clearly the dominant broadening mechanism. The temperature dependence of ΔH is adequately accounted for by considering the effects of uniform magnetic dilution in the region $kT \lesssim J$. Both the local field contributions to the second moment and the spin correlations are changed from their high-temperature values. The EPR data also suggest the presence of magnetically nonequivalent chains in $Cu(C_2O_4)\cdot{}^1/_3H_2O$, with an interchain exchange interaction in the range $0 < zJ' \lesssim 4$ cm^{-1}.

Acknowledgment. We thank R. C. Hughes of Sandia Laboratories for the Q-band measurements and his continued interest in this work. We also thank W. E. Hatfield for access to unpublished susceptibility data. The financial support of the National Science Foundation (Grant GP-4302) is gratefully acknowledged.

Registry No. $Cu(C_2O_4)$, 814-91-5.

References and Notes

(1) (a) L. S. de Jongh and A. R. Miedema, *Adv. Phys.*, **23**, 1 (1974); (b) W. E. Hatfield, *ACS Symp. Ser.* **No. 5** (1974); (c) K. T. McGregor, D. B. Losee, and W. E. Hatfield, *Inorg. Chem.*, **13**, 756 (1974).
(2) (a) B. Bleaney and K. Bowers, *Proc. R. Soc. London, Ser. A*, **214**, 451 (1952); (b) G. Kokoszka and R. W. Duerst, *Coord. Chem. Rev.*, **5**, 209 (1970); (c) K. T. McGregor, D. J. Hodgson, and W. E. Hatfield, *Inorg. Chem.*, **15**, 421 (1976); (d) B. Morosin, R. C. Hughes, and Z. G. Soos, *Acta Crystallogr., Sect. B*, **31**, 762 (1975).
(3) (a) M. Data, H. Yamazaki, M. Motokawa, and S. Tazawa, *Prog. Theor. Phys.*, **465**, 194 (1970); M. Data, M. Motokawa, H. Hori, S. Kuroda, and K. Matsui, *J. Phys. Soc. Jpn.*, **39**, 257 (1975); (b) I. Yamada and M. Ikebe, *ibid.*, **33**, 1334 (1972).
(4) K. T. McGregor and Z. G. Soos, *J. Chem. Phys.*, **62**, 2506 (1976).
(5) T. Moriya, *Phys. Rev.*, **120**, 91 (1960).
(6) For reviews of EPR in low-dimensional systems see, for example, H. J. Keller, Ed., "Low Dimensional Cooperative Phenomena", Plenum Press, New York, N.Y., 1975: (a) Z. G. Soos, p 45; (b) P. M. Richards, p 147; (c) G. F. Kokoszka, p 171.
(7) (a) B. N. Figgis and D. J. Martin, *Inorg. Chem.*, **5**, 100 (1966); (b) L. Dubicki, C. M. Harris, E. Kokot, and R. L. Martin, *ibid.*, **5**, 93 (1966); (c) V. V. Zelenstov and T. G. Aminov, *Dokl. Akad. Nauk SSSR*, **158**, 1393 (1964).
(8) (a) R. Kubo and K. Tomita, *J. Phys. Soc. Jpn.*, **9**, 888 (1954); (b) P. W. Anderson and P. R. Weiss, *Rev. Mod. Phys.*, **25**, 269 (1953); (c) R. Kubo in "Fluctuation, Relaxation and Resonance in Magnetic Systems", D. ter Haar, Ed., Plenum Press, New York, N.Y., 1962; (d) A. Abragam, "Principles of Nuclear Magnetism", Oxford University Press, London, 1961, Chapters IV and X.
(9) Z. G. Soos, *J. Chem. Phys.*, **46**, 4284 (1967).
(10) (a) P. L. Nordio, Z. G. Soos, and H. M. McConnell, *Annu. Rev. Phys. Chem.*, **17**, 237 (1966); (b) K. T. McGregor and W. E. Hatfield, *J. Chem. Phys.*, **62**, 2911 (1975).
(11) (a) P. Pincus, ref 6, p 1; (b) M. E. Fisher, *Am. J. Phys.*, **32**, 343 (1964); (c) F. B. McLean and M. Blume, *Phys. Rev. B*, **7**, 1149 (1973).
(12) J. C. Bonner and M. E. Fisher, *Phys. Rev.* [*Sect.*] *A*, **135**, 640 (1964).
(13) M. T. Hutchings, G. Shirane, R. J. Birgeneau, and S. L. Holt, *Phys. Rev. B*, **5**, 1999 (1972).
(14) (a) F. Carboni and P. M. Richards, *Phys. Rev.*, **177**, 889 (1969); (b) D. W. Hone and P. M. Richards, *Annu. Rev. Mater. Sci.*, **4**, 337 (1974).
(15) (a) J. E. Gulley, D. Hone, D. J. Scalapino, and B. G. Silbernagel, *Phys. Rev. B*, **1**, 1020 (1970); (b) M. J. Hennessy, C. D. McElwee, and P. M. Richards, *ibid.*, **7**, 930 (1973).
(16) Z. G. Soos, T. Z. Huang, J. S. Valentine, and R. C. Hughes, *Phys. Rev. B*, **8**, 993 (1973); T. Z. Huang and Z. G. Soos, *ibid.*, **9**, 4981 (1974).
(17) R. E. Dietz, F. R. Merritt, R. Dingle, D. Hone, B. G. Silbernagle, and P. M. Richards, *Phys. Rev. Lett.*, **26**, 1186 (1971).
(18) M. Blume and J. Hubbard, *Phys. Rev. B*, **1**, 3815 (1970).

(19) C. G. Windsor, *Proc. Phys. Soc., London*, **91**, 353 (1967); M. DeLeener and P. Resibois, *Phys. Rev.*, **152**, 318 (1966), and references therein.
(20) C. Kittel and E. Abrahams, *Phys. Rev.*, **90**, 238 (1953).
(21) L. Shia and G. F. Kokoszka, *J. Chem. Phys.*, **60**, 1101 (1974).
(22) (a) R. C. Hughes and Z. G. Soos, *J. Chem. Phys.*, **48**, 1066 (1968); (b) B. M. Hoffman and R. C. Hughes, *ibid.*, **52**, 4011 (1970); (c) T. Z. Huang, R. P. Taylor, and Z. G. Soos, *Phys. Rev. Lett.*, **28**, 1054 (1972).
(23) R. W. Jotham, *Chem. Commun.*, 178 (1973).
(24) W. E. Hatfield, private communication.
(25) See for example: J. F. Boas, R. H. Dunhill, J. R. Pilbrow, R. C. Srivastava, and T. D. Smith, *J. Chem. Soc. A*, 94 (1969); P. Kottis and R. Lefebvre, *J. Chem. Phys.*, **39**, 393 (1963); C. P. Poole and H. A. Farach, "The Theory of Magnetic Resonance", Wiley-Interscience, New York, N.Y., 1972.
(26) See for example B. J. Hathaway and D. E. Billing, *Coord. Chem. Rev.*, **5**, 143 (1970).

Contribution from the Department of Chemistry, University of Ottawa, Ottawa, Canada, K1N 6N5

Oxofluoro Complex Anion Equilibria in Aqueous Hydrofluoric Acid. 3. Iodate(V) in Concentrated Hydrofluoric Acid (>26 M)

JOHN B. MILNE* and DUNCAN M. MOFFETT

Received January 7, 1976 AIC60005E

The vibrational spectra of the IOF_4^- anion in $CsIOF_4$ and $KIOF_4$ and in solution in CH_3CN have been determined and assigned. Solutions of various ratios of IF_5 and H_2O in CH_3CN and of HIO_3 in hydrofluoric acid (48–100%) have been studied by Raman and ^{19}F NMR spectroscopy. The spectra of the acetonitrile solutions with up to a nearly equimolar ratio of H_2O to IF_5 are consistent with the presence of, in addition to the IOF_4^- ion, $HIOF_4$ and IF_5, while the spectra of the hydrofluoric acid solutions show the presence of $IO_2F_2^-$ ion, HIO_2F_2, $HIOF_4$, and IF_5.

Introduction

Recently the results of two studies of the behavior of iodine(V) in hydrofluoric acid have been reported.[1,2] El-Gad and Selig[1] showed that IF_5 is formed when I_2O_5 or $NaIO_3$ is dissolved in anhydrous HF. These authors found no evidence for the IF_6^- ion or for other oxofluoro or hydroxofluoro species in their solutions. Milne and Moffett[2] studied solutions of HIO_3 in aqueous hydrofluoric acid (<26 M) and found evidence for the species HIO_3, IO_3^-, and $IO_2F_2^-$. They evaluated the constant governing the equilibrium between IO_3^- and $IO_2F_2^-$. The region of HF concentration between 48 and 100% has not been thoroughly studied and forms the subject of this paper. Of particular interest was the possible existence of the IOF_4^- ion in these solutions. Compounds with this anion have been particularily elusive[3] although the x-ray crystal structure of $CsIOF_4$ has been reported[4] and the anion is a likely impurity in the preparations of hexafluoroiodate(V) compounds.[5,6]

Experimental Section

Materials. Iodic acid, 99% (BDH), potassium iodate (BDH), potassium fluoride, 98% (BDH), and cesium fluoride, 99% (Ozark-Mahoning), were dried by heating under vacuum for 12 h before use; hydrofluoric acid, 48% (J. T. Baker), was standardized against standard NaOH using phenolphthalein indicator before use. Anhydrous grade HF (Matheson) was used directly. Iodine pentafluoride, 98% (Matheson), was purified by distillation from NaF to remove HF and then from Hg to remove I_2. The distillation was carried out under vacuum in an all-glass break-seal apparatus. Acetonitrile, anhydrous (Eastman), was purified by distillation from P_2O_5.

Cesium iodate was prepared by crystallization from an aqueous solution of Cs_2CO_3 and HIO_3. Potassium difluoroiodate was prepared by the method of Helmholz and Rogers.[7] Three methods were tried for the preparation of the M^IIOF_4 compounds: (1) from a stoichiometric mixture of M^IIO_3, MF (M^I = K, Cs), and IF_5 according to the reaction

$$M^IIO_3 + 2M^IF + 2IF_5 = 3M^IIOF_4$$

(2) from a stoichiometric mixture of KIO_2F_2, KF, and IF_5 according to the reaction

$$KIO_2F_2 + KF + IF_5 = 2KIOF_4$$

and (3) by hydrolysis of hexafluoroiodate in acetonitrile

$$M^IIF_6 + H_2O = M^IIOF_4 + 2HF$$

Reactions were carried out in all-glass apparatus and transfers were done in a drybox. All of the methods produced M^IIOF_4 as indicated by ir spectra of the products, which showed the characteristic IO stretching mode of the IOF_4^- ion at 890 cm^{-1},[3,4] but none of the products was completely free of $M^IIO_2F_2$ impurity with moderately strong ir bands at 805–815 cm^{-1}.[2,8] Both acetonitrile and IF_5 were used as solvents for methods 1 and 2, but where the latter was used as solvent, an ir spectrum of the product showed that M^IIF_6, with characteristic bands in the region 605–655 cm^{-1},[5,9] was present. Neither $M^IIO_2F_2$ nor M^IIOF_4 produces bands in this spectral region. Recrystallization from acetonitrile gave a product which was free of M^IIF_6 but which consisted of $M^IIO_2F_2$ and M^IIOF_4.

Ryan and Asprey[4] obtained crystals of $CsIOF_4$ from a mixture of CsI and IF_5 in acetonitrile. The oxygen source was not identified and could be either the glass reaction container itself or water adsorbed on the surface of the glass. It is interesting that XeF_6 reacts with Pyrex glass to give $XeOF_4$[10] and a similar reaction may occur with the isoelectronic IF_6^- ion: $2IF_6^- + SiO_2 = 2IOF_4^- + SiF_4$. To test this possibility a preparation of KIF_6 in CH_3CN was carried out in the presence of finely ground glass, which had been dried under vacuum, but the ir spectrum of the product showed only the presence of KIF_6 and SiO_2 in the product.

A typical preparation had 2.94 g of KF (0.05 mol), 5.41 g of KIO_3 (0.025 mol) and 11.15 g of IF_5 (0.05 mol). The mixture was shaken in 50 ml of dry acetonitrile for 24 h and then pumped dry under vacuum. The ir spectrum of the product could be accounted for by the presence of only KIO_2F_2 and $KIOF_4$. Anal. Calcd for $KIOF_4$: I, 49.19. Calcd for $KIOF_4$ containing 8% KIO_2F_2: I, 49.65. Found: I, 49.65. All products were analyzed for fluoride by titration with $La(NO_3)_3$, using a fluoride-sensitive electrode. Reasonably sharp end points were observed but the results were shown subsequently to be 15–20% high.[2] Using a correction factor of 0.85 estimated from the analysis of $M^IIO_2F_2$ compounds,[2] the fluoride content of the $KIOF_4$ product above was found to be 28% (calcd for $KIOF_4$, 29.46%; calcd for $KIOF_4$ containing 8% KIO_2F_2, 28.40%).

Methods. Analysis. Iodine was determined as iodate by reduction with excess KI and titration of liberated iodine with thiosulfate. The fluoride analysis has been discussed elsewhere.[2]

Spectroscopy. Ir spectra were taken as mulls in Nujol with CsBr plates using a Beckman IR20A spectrometer. Band positions were accurate to ±5 cm^{-1}. Raman spectra were taken on a Jarrell-Ash 300 spectrometer. All spectra were taken at 25 °C. The 4880-Å line of a Spectra Physics argon ion laser was used to excite the spectra and detection was by a cooled photomultiplier tube. A spike filter